Friction Stir Welding of Dissimilar Aluminium Alloys

R. Braun, U. Alfaro Mercado, C. Dalle Donne

German Aerospace Center (DLR), Institute of Materials Research, D-51170 Cologne, Germany

Keywords: Friction stir welding, AA6056, AA2024, hardness, tensile strength, corrosion behaviour, galvanic coupling, intergranular corrosion, stress corrosion cracking

Abstract

The friction stir welding process was used to produce dissimilar butt joints of 4 mm thick sheet of the aluminium alloys 2024-T351 and 6056-T651. A tensile strength of 278 MPa was measured for the dissimilar friction stir welds in the as-welded condition. Fracture occurred in the heat affected zone of alloy 6056 correlating with the minimum in the hardness profile. The corrosion performance of the dissimilar joints observed in the various immersion tests was governed by galvanic coupling of the different aluminium alloys. Being more active, alloy 6056-T651 provided cathodic protection to 2024-T351 when exposed to aqueous chloride solutions, particularly under permanent immersion conditions. The heat affected zone of 2024 was sensitive to intergranular corrosion. Applying tensile stresses, intergranular corrosion could be accelerated resulting in environment-induced cracking in this region.

1. Introduction

In new aircraft design such as for the A380, integrally stiffened structures are considered to reduce manufacturing costs and weight [1]. Welding is an important joining technique for advanced metal structures, replacing conventional riveting and bonding processes used in current airframe components [2]. Besides laser beam welding, friction stir welding (FSW) has gained increasing importance as joining technique in fuselage and wing applications [3]. Being a solid state process, FSW is an appropriate technique to join wrought aluminium alloys with thickness ranging from 0.5 to 75 mm, including alloys which are regarded as difficult to weld by fusion processes [4]. Combinations of different metals in components provide a great flexibility in design and production and an optimised use of material properties. The FSW technique has the potential to weld dissimilar metals, in particular different aluminium alloys. The objective of the present work was to join the dissimilar aluminium alloys 2024 and 6056 using the FSW technique. Besides on tensile properties, the investigation has focused on the corrosion behaviour of dissimilar friction stir welds with regard to galvanic coupling.

2. Experimental

The materials used were 4 mm thick unclad sheet of the alloys 2024-T351 and 6056-T651. Butt welds of dissimilar aluminium alloys were produced using the friction stir welding technique on the basis of the TWI patent [5]. Alloy 2024-T351 was placed at the retreating side of the joint. The welding direction was parallel to the rolling direction of the parent sheet. Tool rotational speed and travel speed were 1200 rpm and 300 mm/min, respectively. Vickers hardness measurements were performed on etched metallographic sections of the welds along the half thickness line with a load of 9.81 N. Tensile tests were carried out using transverse oriented flat tensile specimens with a gauge length of 50 mm and a width of 12 mm. Susceptibility to intergranular corrosion was evaluated performing immersion tests according to ASTM G110. Coupons with a size of 25 by 50 mm were exposed to an aqueous chloride-peroxide solution for 6 h. Weld face and weld root sides were investigated. The exfoliation corrosion behaviour was studied performing EXCO tests (ASTM G34) and modified salt spray tests (ASTM G85, Annex 2). Panels used were 50×100 mm in size. The stress corrosion cracking behaviour was studied using four-point loaded bent beam specimens (ASTM G39) being 30 mm wide and 205 mm long. The thickness was reduced to 2 mm by milling one side. For both weld face and weld root sides, triplicate bent-beam specimens were alternately immersed in 3.5% NaCl solution (ASTM G44) for a maximum exposure time period of 1000 h. At the maximum bending deflection chosen, the applied stress in transverse direction was 180 and 190 MPa for the alloys 6056 and 2024, respectively, depending on the elastic moduli.

3. Results and Discussion

Metallographic examinations of the dissimilar 2024/6056 joints revealed a nugget with ring pattern formed by the flow and mixing of the material from the two sides (Fig.1a). Bonding between the material strips was intimate, but mixing of the two alloys with regard to their chemical composition was highly inhomogeneous. The nugget exhibited a fine equiaxed grain structure for both alloys. In the adjacent thermomechanically affected zones, grains of the parent materials were plastically deformed. The hardness profile across the weld is presented in Fig. 1b, taken in the mid-section of the joint. The lowest values were measured in the heat affected of alloy 6056. Because the hardness dropped below the 6056-T4 level (~105 HV1), this region was probably overaged. To join dissimilar alloys, welding parameters diverged from those being optimised for welding same alloys, generating a too high heat input for alloy 6056. Tensile properties measured for dissimilar friction stir welds in transverse direction were: yield strength = (228 ± 5) MPa, ultimate tensile strength = (278 ± 5) MPa, fracture elongation = (1.6 ± 0.1) %. Failure occurred in the heat affected zone of alloy 6056. The low fracture elongation was associated with inhomogeneous straining within the 50 mm gauge length used. Local ductility was high, as confirmed by fractography showing a ductile dimple-like shear fracture.

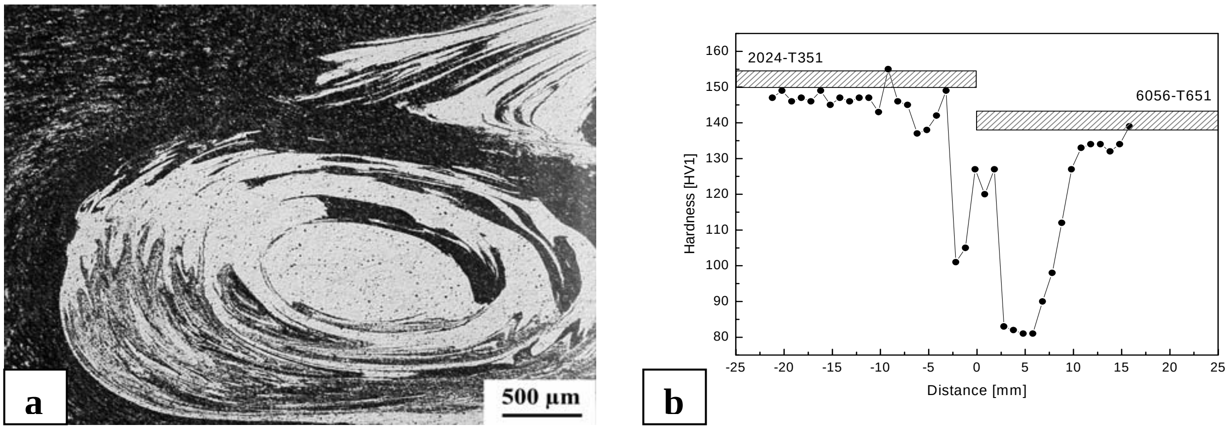

Figure 1: Metallographic section of the nugget (a) and hardness profile across the weld (b) of a dissimilar 2024/6056 FSW joint.

Table 1: Corrosion potentials (in mV_{NHE}) of the base alloys 2024 and 6056 in different tempers, measured according to ASTM G69.

2024-T351	2024-T851	6056-T451	6056-T651
-362	-480	-453	-506

Corrosion potentials measured according to ASTM G69 are listed in Table 1 for the base alloys 2024 and 6056 in different tempers. When exposed to an aqueous chloride-peroxide solution, alloy 2024-T351 was found to be the most noble metal. With increasing aging the corrosion potentials of both alloys shifted to more active values.

When immersed in an aqueous chloride-peroxide solution according to ASTM G110, the base alloys 2024-T351 and 6056-T651 were sensitive to intergranular corrosion and pitting corrosion, respectively. Maximum depths of attack measured in metallographic sections were 200 µm for 2024-T351 and 110 µm for 6056-T651. The corrosion behaviour of dissimilar friction stir welds depended primarily on galvanic coupling effects due to the different chemical compositions and microstructural changes caused by the frictional heat. Being in contact with 2024-T351, alloy 6056-T651 was more active, as indicated by the corrosion potentials listed in Table 1. Thus, alloy 6056-T651 provided cathodic protection to the more noble metal of the dissimilar joint. Accordingly, metallographic examinations of welded coupons revealed enhanced pitting corrosion with the 6056-T651 part (maximum depths of attack were 280 and 225 µm at the weld face and weld root sides, respectively), whereas a significantly reduced intergranular corrosion attack was found for the 2024-T351 part (maximum depths were 30 µm at the weld face side and 65 µm at the weld root side). In the fine grain area of the weld region, 6056 strips suffered pitting and intergranular corrosion. Similarly, alloy 6056 exhibited galvanic corrosion near the bonding line of the two alloys at the weld root side (Fig 2a). In comparison to the base material, intergranular corrosion observed in the heat affected zone of alloy 2024 at the weld face side was more severe than that found with the base alloy (Fig. 2b). The maximum depth of attack measured was 360 µm. The enhanced intergranular corrosion susceptibility might be associated with quench sensitivity of alloy 2024 resulting in solute precipitation as coarse particles of the equilibrium phase. This loss of solute might shift the corrosion potential of the heat affected zone to more negative values preventing cathodic protection by alloy 6056. A similar change of the corrosion potential might be caused by the heat input of the FSW process resulting in an artificially aged microstructure of alloy 2024 in this region. As given in Table 1, the corrosion potential of 2024-T851 was more active than that of 6056-T451 corresponding to the microstructure of alloy 6056 in the nugget region.

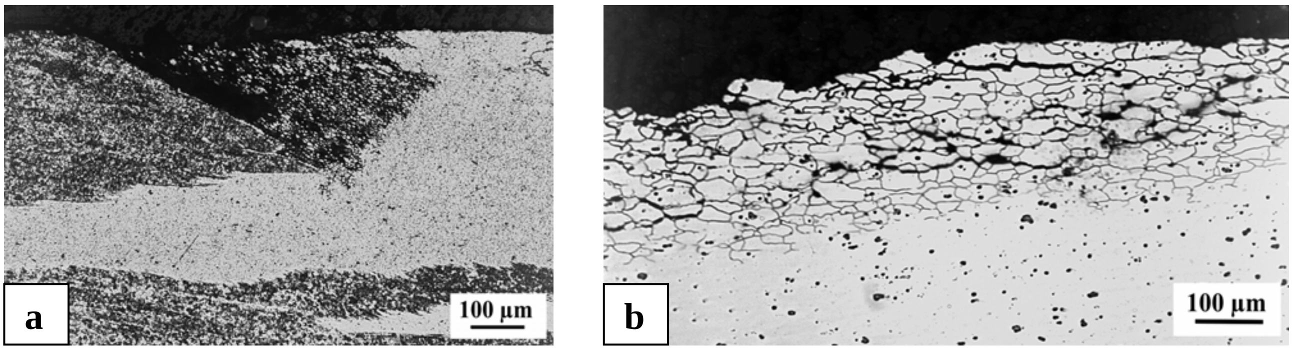

Figure 2: Metallographic sections of coupons of dissimilar FSW joints which were immersed in an aqueous chloride-peroxide solution for 6 h, showing (a) galvanic corrosion of alloy 6056 adjacent to the bonding line of the two alloys at the weld root side (a) and intergranular corrosion in the heat affected zone of alloy 2024 (b).

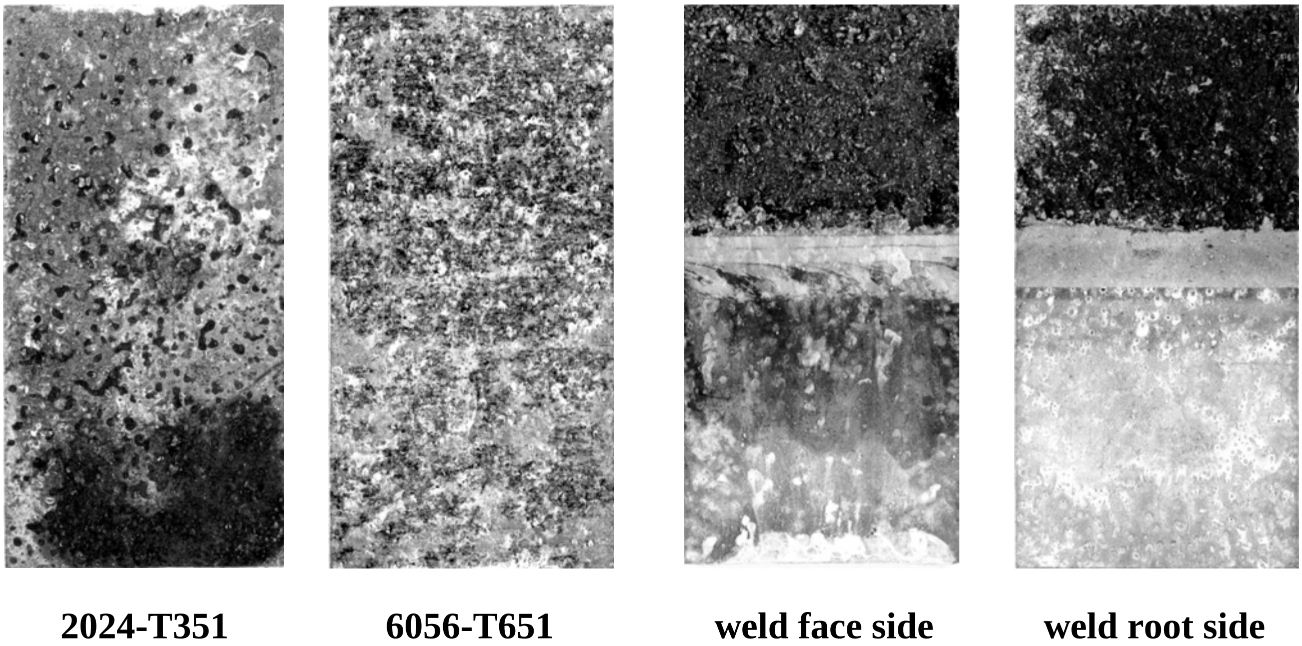

Figure 3: Appearance of panels of the base alloys and dissimilar FSW joints after 96 h exposure to the EXCO solution (6056-T651 part of the dissimilar joints is on the top of the panels being 50×100 mm^2 in size).

Surface appearance of panels after 96 h exposure to the EXCO solution is shown in Figure 3. Both base materials exhibited blistering. Alloy 6056-T651 was slightly more corroded revealing blisters mainly split open. Slight uniform corrosion was observed on the 2024-T351 part of dissimilar joints, whereas the 6056-T651 part suffered severe exfoliation corrosion. A considerable amount of loose exfoliation products was found lying on the bottom of the container. Therefore, severity of exfoliation corrosion was rated EC/ED according to ASTM G34. The fine grain area on the weld face side was not attacked by localized corrosion. At the weld root side, an about 10 mm wide zone being free of corrosion was observed on the 6056 part adjacent to the bonding line. The microstructure of this region was probably in a naturally aged condition. When immersed in the EXCO solution, the 6056-T651 part of the dissimilar joints seemed to be the most active metal providing cathodic protection to the remaining area of the panels.

Figure 4 shows the surface appearance of panels of the base alloys and dissimilar joints after 2 weeks of cyclic acidified salt spray testing. The base alloys 6056-T651 and 2024-T351 suffered pitting and exfoliation corrosion with rating EB, respectively. Panels of dissimilar friction stir welds exhibited also pitting and exfoliation corrosion (EB) on the 6056-T651 and 2024-T351 parts being similar to the corrosion attack found with the base alloys. In the weld region, the corrosion attack depended upon alloy composition and heat treatment condition. On the weld face side, regions of alloy 6056 within the fine grain area corroded by pitting. A similar corrosion attack was found with alloy 6056 near the bonding line at the weld root side. The heat affected zone of alloy 2024 exhibited exfoliation corrosion with rating EB and blistering on the weld face and weld root sides, respectively. Adjacent to the heat affected zone, an about 10 mm wide band without corrosion attack was found on both weld sides. Beyond this, alloy 2024-T351 suffered exfoliation corrosion. Again, alloy 6056-T651 seemed to be the most active metal of the dissimilar 2024/6056 joint when exposed to the acidified salt spray fog. However, due to the cyclic testing procedure (drying and soaking periods) cathodic protecting of alloy 6056-T651 was less effective, resulting in exfoliation corrosion of the heat affected zone of alloy 2024 and even of the 2024-T351 part at a sufficiently large distance between both parent sheets.

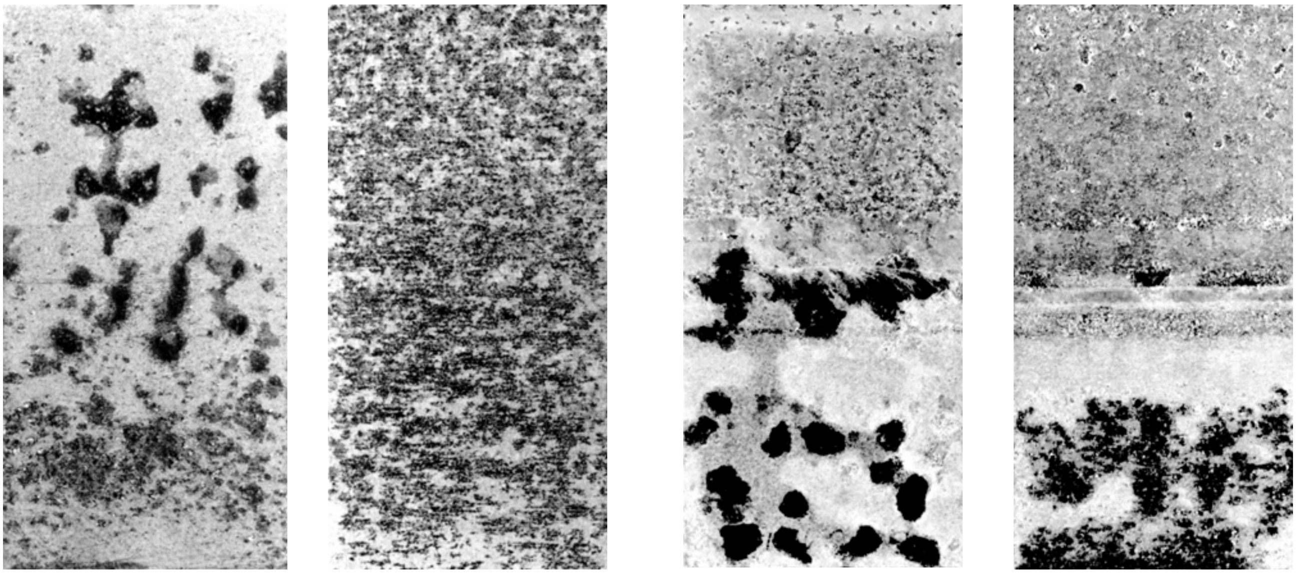

2024-T351 **6056-T651** **weld face side** **weld root side**

Figure 4: Appearance of panels of the base alloys and dissimilar FSW joints after 2 weeks of exposure to an intermittent acidified salt spray fog (6056-T651 part of the dissimilar joints is on the top of the panels being 50×100 mm^2 in size).

Dissimilar 2024/6056 FSW joints were basically resistant against stress corrosion cracking at applied stresses up to 180 MPa. Five of six bent-beam specimens did not fail during a 1000 h exposure to 3.5% NaCl solution under alternate immersion conditions. One specimen with weld face side being tested failed after 30 days of exposure. Fractographic examinations revealed an intergranular fracture with dissolved grain boundaries (Fig. 5a). The dissolution of grain boundaries could result from the environmentally assisted cracking mechanism being operative (anodic dissolution), but also from a post-fracture attack. Metallographic examinations of bent-beam specimens of dissimilar joints, which were alternately immersed in 3.5 % NaCl solution for 1000 h, revealed pitting for the 6056-T651 part (155 µm maximum pit depth) and pitting and intergranular corrosion for the 2024-T351 part (550 µm maximum depth of attack). The corrosion attack was aggravated in the heat affected zone of both alloys. At the bonding lines between both materials, alloy 6056 corroded again preferentially under this environmental condition, but severity of corrosion due to galvanic coupling was reduced in comparison to that found under permanent immersion condition in an aqueous chloride-peroxide solution. Cathodic protection of the more noble metal 2024-T351 was not observed. Fine grain areas of alloy 6056 in the weld region suffered pitting and intergranular corrosion with a maximum depth of 450 µm. The most severe degradation of dissimilar 2024/6056 FSW joints occurred in the heat affected zone of alloy 2024 caused by a predominantly intergranular corrosion attack penetrating up to 730 µm (Fig. 5b). Therefore, environment-induced cracking observed for one bent-beam specimen was probably caused by stress assisted intergranular corrosion.

4. Conclusions

- Dissimilar joints of 4 mm thick sheet of the aluminium alloys 2024-T351 and 6056-T651 were successfully produced using the FSW technique.
- A deep hardness drop was found in the heat affected zone of alloy 6056.

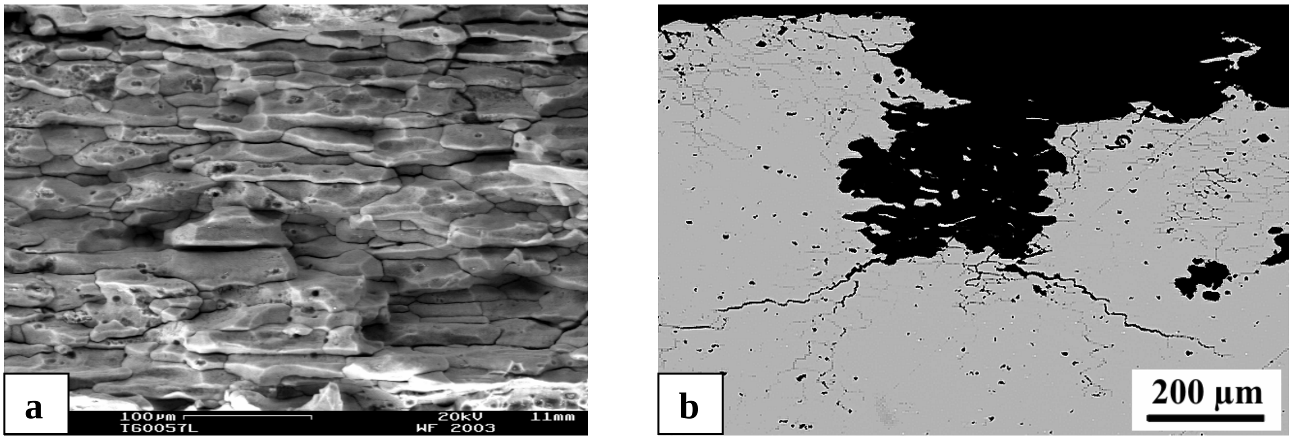

Figure 5: Fractographic (a) and metallographic (b) examinations of bent-beam specimens of dissimilar 2024/6056 FSW joints which were alternately immersed in 3.5% NaCl solution, showing (a) intergranular fracture (specimen failed after 30 days of exposure) and (b) pitting and intergranular corrosion in the heat affected zone of alloy 2024.

- Strength of the dissimilar friction stir welds in the as welded condition approached 75 % of the ultimate tensile strength of the base alloy 6056-T651. Fracture occurred in the heat affected zone of alloy 6056.
- The corrosion behaviour of dissimilar friction stir welds immersed in an aqueous chloride-peroxide solution was controlled by galvanic coupling. Being more active, alloy 6056-T651 provided cathodic protection to alloy 2024-T351. The heat affected zone of alloy 2024 suffered intergranular corrosion.
- When immersed in the EXCO solution, the 6056-T651 part of the dissimilar joints suffered severe exfoliation corrosion, whereas the 2024-T351 part did not exhibit localised corrosion.
- Intermittent acidified salt spray testing indicated moderate exfoliation corrosion and pitting for the 2024-T351 and 6056-T651 parts, respectively. In the weld region, alloy 6056 suffered galvanic corrosion. The heat affected zone of alloy 2024 was susceptible to exfoliation corrosion.
- When alternately immersed in 3.5% NaCl solution, the heat affected zone of alloy 2024 was found to be quite sensitive to intergranular corrosion. At applied tensile stresses exceeding 180 MPa, dissimilar friction stir welds could fail in this region by stress assisted intergranular corrosion.

Acknowledgement

The authors wish to thank the European Community for funding this work within the 5th Framework Programme WAFS (GRD1-199-1027).

References

[1] H.-J. Schmidt, B. Schmidt-Brandecker, N. Ohrloff, and T. Fleischer, ICAF ’99, Vol. 1, edited by J. L. Rudd and R.M. Bader, EMAS, Cradley Heath, 537-552, 1999.

[2] W. Zink, Advanced Aerospace Materials, edited by M. Peters and W.A. Kaysser, Deutsche Gesellschaft für Luft- und Raumfahrt e.V., Bonn, 25-32, 2001.

[3] S.W. Kallee, W.M. Thomas, and E.D Nicholas, Advanced Aerospace Materials, edited by M. Peters and W.A. Kaysser, Deutsche Gesellschaft für Luft- und Raumfahrt e.V., Bonn, 33-40, 2001.

[4] W.M. Thomas, K. I. Johnson, C.S. Wiesner, Advanced Engineering Materials, 485-490, 2003.

[5] W.M. Thomas, E.D. Nicholas, J.C. Needham, M.G. Murch, P. Temple-Smith, and C.J. Dawes, EU Patent 0 615 480 B1, 1992.